Observations of drizzle in nocturnal marine stratocumulus

M.C. VANZANTEN, *

Department of Atmospheric Sciences,
University of California Los Angeles, Los Angeles, California, USA
and
Institute of Marine and Atmospheric Research Utrecht,
Utrecht University, Utrecht, The Netherlands

B. STEVENS

Department of Atmospheric Sciences,
University of California Los Angeles, Los Angeles California, USA

G. VALI

Department of Atmospheric Science
University of Wyoming, Laramie Wyoming, USA

D. H. LENSCHOW

National Center for Atmospheric Research
Boulder Colorado, USA

Submitted to the *Journal of Atmospheric Sciences* 6 October, 2003.

ABSTRACT

In situ and radar data from the second field study of the dynamics and chemistry of marine stratocumulus (DYCOMS-II) have been used to study drizzle in stratocumulus. Our measurements indicate that drizzle is prevalent. During five of seven analyzed flights precipitation was evident at the surface, and on roughly a third of the flights mean surface rates approached or exceeded 0.5 mm d^{-1}. Additional analysis of the structure and variability of drizzle indicates that the macroscopic (flight averaged) mean drizzle rates at cloud base scale with H^3/N where H is the flight averaged cloud depth and N the flight averaged cloud droplet number concentration. To a lesser extent flight-to-flight variability in the mean drizzle rate also scales well with differences in the 11 and 4 micron brightness temperatures, and the cloud top effective radius. The structure

**Corresponding Author Address:* Institute of Marine and Atmospheric Research Utrecht, Utrecht University, Princetonplein 5, 3584 CC Utrecht, The Netherlands. Email: M.C.vanZanten@phys.uu.nl.

of precipitating stratocumulus boundary layers is also investigated, and a general picture emerges of large flight averaged drizzle rates being manifested primarily through the emergence of intense pockets of precipitation. The characteristics of the drizzle spectrum in precipitating versus non precipitating regions of a particular cloud layer were mostly distinguished by the number of drizzle drops present, rather than a change in size of the median drizzle drop, or the breadth of the drizzle spectrum.

1. Introduction

Among the pantheon of processes involving stratocumulus, drizzle occupies a peculiar place. Despite observational evidence that it is commonplace, it is conspicuously absent in most of our conceptual and theoretical descriptions of stratocumulus.

Already during the late 1970s and early 1980s measurements in stratocumulus (Brost et al. (1982) and Nicholls (1984); Nicholls and Leighton (1986)) showed that at times the drizzle flux contributes significantly to the total water budget. Nicholls (1984) for instance showed that the gravitational settling of drizzle drops was commensurate with the turbulent flux, through the entire boundary layer, not just inside the cloud. Similar results were derived from an analysis of data collected during ASTEX (*e.g.*, Duynkerke et al. (1995), Frisch et al. (1995) and Bretherton et al. (1995)) and FIRE (Austin et al. 1995) and can be inferred from measurements during SOCEX (Boers et al. (1996) and Boers et al. (1998)) and data from an experiment off the coast of Oregon (Vali et al. 1998). In this paper, we present evidence from data collected during the Dynamics and Chemistry of Marine Stratocumulus -II field study (DYCOMS-II) that drizzle may be even more prevalent than previously thought. In only two of the seven flights was there no evidence of drizzle at the sea surface and in two of the flights drizzle rates were substantial, making drizzle something more of a rule than an exception.

Despite the observational record, in the modeling community drizzle is often neglected or treated marginally (see *e.g.*, the stratocumulus cases simulated by the GCSS working group 1 (Duynkerke et al. 1999)). Of existing drizzle modeling work, most is concerned with either the formation of drizzle (*e.g.*, Nicholls (1987), Feingold et al. (1996), Austin et al. (1995)) or the influence of turbulence on the microphysics of stratocumulus clouds (Kogan et al. 1995). Both types of studies have a distinct microphysical perspective. Cloud macroscopic features and their relation to drizzle are less often studied. The feedback of drizzle on the cloud dynamics has been dealt with in some one dimensional modeling studies (*e.g.*, Albrecht (1989), Ackerman et al. (1993), Pincus and Baker (1994), Chen and Cotton (1987), Wang and Wang (1994)), in which of course most of the important processes have to be parameterized. Stevens et al. (1998) is one of a few studies so far to utilize large eddy simulation to study how drizzle interacts with the turbulent structure of the PBL. By and large all of these studies provide support for the idea that drizzle can regulate cloudiness in important ways.

But in our theoretical development of the subject, the role of drizzle as trait d'union between cloud microphysics and cloud dynamics is still somewhat overlooked. Is this warranted? Should we think of drizzle as being an important process but yet of secondary significance so that neglecting it is justified? Or is drizzle inextricably bound up with the life cycle of stratocumulus as is suggested in *e.g.*, Paluch and Lenschow (1991)? Influencing the lifespan of stratocumulus would give drizzle an important role in the climatology of stratocumulus fields and thus indirectly affect the radiative balance of the Earth as well. Because it is suggested that larger aerosol concentrations negatively influence the amount of precipitation, this would lead to a direct way in which man modifies the climate of the Earth (*e.g.*, Albrecht (1989) and Pincus and Baker (1994)). To address these issues simple drizzle parameterizations are being formulated for general circulation models (*e.g.*, Khairoutdinov and Kogan (2000)). However these parameterizations are generally being implemented without a clear idea of how drizzle contributes to the existing stratocumulus

flight	$\langle R \rangle$ [mm d^{-1}]
RF01	BDL
RF02	0.35 ± 0.11
RF03	0.05 ± 0.03
RF04	0.08 ± 0.06
RF05	BDL
RF07	0.60 ± 0.18
RF08	0.12 ± 0.03

Table 1: Average drizzle rates $\langle R \rangle$ (BDL denotes below detection limit) for each flight at 70 m height above the sea surface based on radar data. Each value represents roughly five hours of data. The conversion from radar reflectivity to drizzle rate is done with Z-R relationships derived from *in situ* instruments (SPP-100 and 260X) for each individual flight (RF02, RF03, RF04, RF07, RF08) or a Z-R relationship derived for all night flights (RF01 and RF05). For information on the specified uncertainty see section 3 a. and 5..

climatology, nor how it interacts with other processes, such as turbulent mixing and entrainment.

For these reasons we believe that a better quantification of the role of drizzle is necessary. Data collected during DYCOMS-II provide a unique opportunity to contribute to such a quantification. During DYCOMS-II a downward looking 95-GHz radar (Vali et al. 1998) was mounted on the NCAR/NSF C130. From this vantage point it was able to collect reflectivity data throughout the cloud layer, and down close to the sea surface almost continuously during the whole time period of each flight, thus creating the possibility to get for the first time an almost continuous estimate of the surface precipitation rate. The outcome of this calculation is presented in Table 1, which shows the prevalence of drizzle during DYCOMS-II. This, and the ability to evaluate its horizontal and vertical structure using both *in situ* and remotely sensed data allow us to go beyond earlier studies (*e.g.*, Austin et al. (1995) and Frisch et al. (1995), both of which had similar objectives but relied on less comprehensive instrumentation). This article is intended to give the reader more background on and in depth understanding of the numbers in Table 1. In section 2. and 3. we discuss how the numbers in Table 1 were estimated. In section 4. we examine the structure behind these numbers, in particular focusing on how drizzle scales with cloud macroscopic features, at what scales drizzle is found, and the nature of its spatial and temporal variability, both within and among flights. We conclude with a discussion and a summary.

2. The DYCOMS-II field study

a. General description

DYCOMS-II took place in July 2001, several hundred kilometers to the west-southwest of San Diego. It consisted of nine flights in stratocumulus topped marine boundary layers. During the experiment favorable conditions were encountered; relatively uniform, and spatially extensive stra-

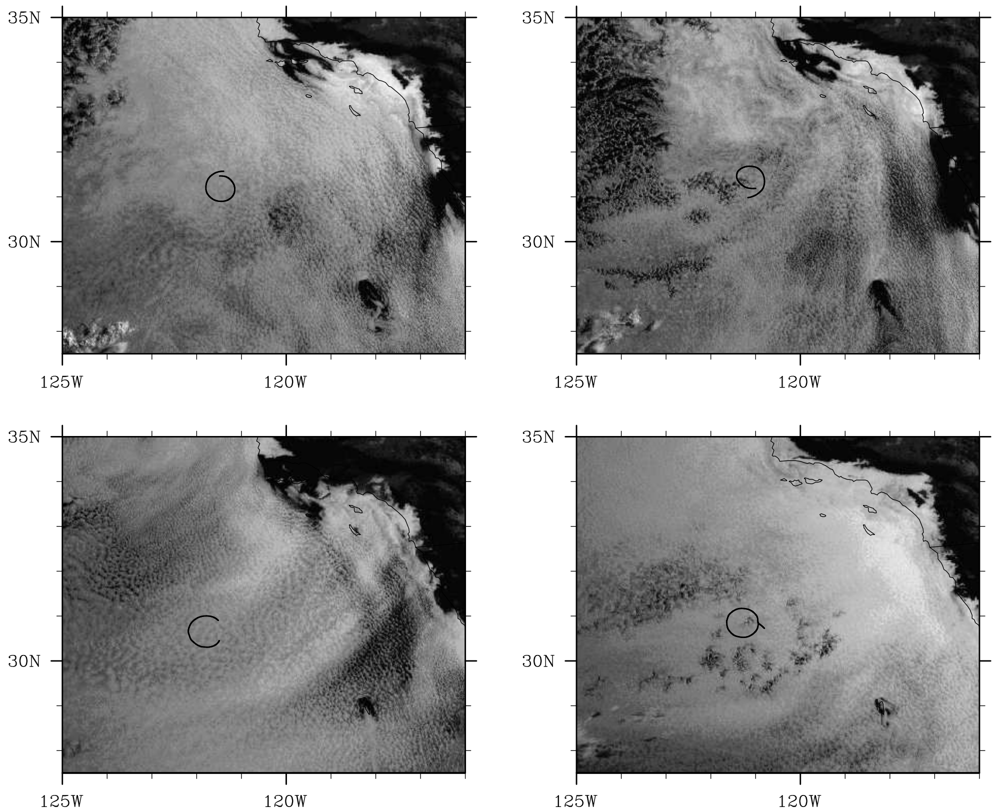

Figure 1: Channel 1 reflectances from GOES-10 for RF01 (upper left panel), RF02 (upper right panel), RF05 (lower left panel) and RF07 (lower right panel). All pictures are first light images (14.30 UTC) with the circles denoting the location of the last leg which were more or less coincidence with the time of the snapshot.

tocumulus cloud decks were probed with almost no breaks or clearings along the flight path. In Figure 1 we present satellite images of four of the nine flights, two flights without drizzle reaching the surface and two flights with high values of surface drizzle rates, $\langle R \rangle$. Besides showing the uniformity of the cloud layers on the scale of a measurement segment (circles of roughly 60 km diameter) the Figure also shows that the non-drizzling cases have a more uniform appearance on the large scale than the more heavily drizzling flights (Stevens et al. 2003b, e.g.,).

One of the initial surprises of DYCOMS-II was the variability in radar derived cloud microstructure among flights. For instance, regions of vigorous drizzle (10 mm d^{-1} or more) were quite common during several flights, on other flights drizzle rarely was seen below cloud base. Figure 2 encapsulates some of this variability. The differences between the structure of the non-precipitating cloud in RF01 and its precipitating counterpart observed during RF07 are striking. (Note the change in scale, where 10 dBz corresponds to roughly an order of magnitude difference in drizzle rate.) A curtain-like echo pattern is visible during RF07, with radar reflectivities almost constant with height in places, and drizzle extending to the sea surface almost everywhere. Superimposed are local cells or pockets with significantly enhanced reflectivities, indicative of much

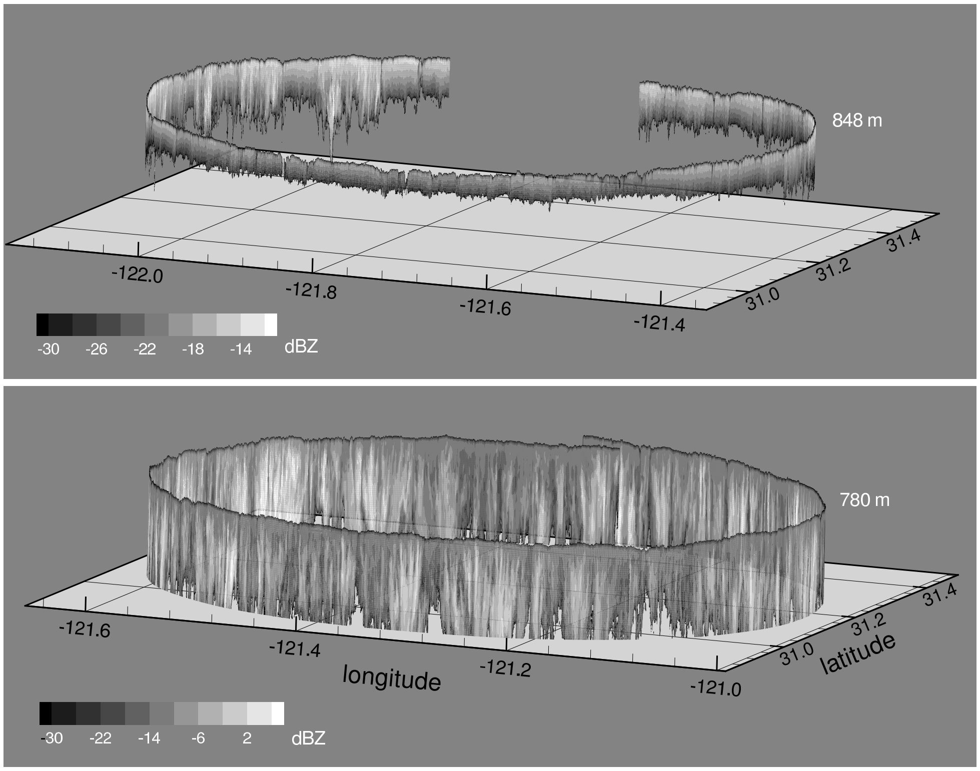

Figure 2: Radar reflectivity of the clouds looking down from above during RF01 (upper panel, 11:46 - 12:15 UTC) and RF07 (lower panel, 11:06 - 11:36 UTC). Note that the scale range for both panels is different. The height specified in each panel denotes cloud top height.

higher drizzle rates. In contrast during RF01 radar returns are confined to the cloud layer, with only a few patches of echos extending lower down. The tendency for the reflectivity to increase with height in the cloud in this latter case is consistent with most of the radar returns coming from an adiabatic cloud microstructure, where mean particle sizes increase toward cloud top.

In addition to tantalizing data such as these, several technical issues also make the DYCOMS-II data appealing for further analysis. The most important being the fact that both *in situ* and remotely sensed data are available from which the drizzle rate can be estimated. These different types of data complement each other. Moreover, redundancy in microphysical *in situ* instrumentation allowed for independent estimates of *e.g.*, the *in situ* drizzle rate. Secondly, all but two flights were nocturnal. Stratocumulus clouds are thought to deepen through the night which is a favorable condition for drizzle to occur. Further, because the flight patterns were flown in a Lagrangian way, approximately one single air mass was probed during each flight.

Of the nine research flights flown during DYCOMS-II, we focus on seven. These seven were selected because they all had a similar flight pattern consisting of circles with a radius of 30 km. The long flight legs of $\sim$ 30 min enabled sufficient averaging to reduced sampling uncertainty yet still provided insights into the spatial and temporal variability at each flight level. Usually two of the circles were flown consecutively, but in opposite directions. Within the boundary layer, measurements were concentrated at four levels; at cloud top (CT), just above cloud base (CB), just below cloud base (SC) and near the surface (SF)). In addition to flight segments within the boundary layer, three remote sensing legs (RL) above the boundary layer were flown at the beginning, middle, and end of each flight. The fact that the flight strategy was almost identical for each flight facilitated intercomparison among flights. The latter was especially interesting because the flight dates and targets were specified *a priori*, hence the data sampled the clouds within the general target area in a manner which was not biased by preconceptions of flow patterns or statistics. More detailed information about the flight plan, available instruments, specific aims of the experiment, overviews of each flight and preliminary results can be found in Stevens et al. (2003a).

b. Instrumentation and data quality

The bulk of this paper is based on an analysis of measurements from a small subset of the instrumentation carried on the NSF/NCAR C130 aircraft: the 95 GHz Wyoming Cloud Radar and three instruments for estimating the drop size distribution (DSD); one based upon single-particle scattering and the other two on shadowing of light. These last three instruments had a sample frequency of 10 Hz.

The SPP-100 (an electronically upgraded version of the Forward Scattering Spectrometer Probe, SPP stands for Signal Processing Package) measured the cloud DSD (CDSD) between 2 and 47 μ m divided into 40 size intervals. We combined the SPP-100 data into 19 unequal-sized bins in order to minimize sizing ambiguities. During DYCOMS-II several problems were encountered with the SPP-100. For RF01 and RF02 the data are slightly questionable because it was determined that the instrument was overestimating droplet sizes by approximately two bin sizes. For the remainder of the experiment another SPP-100 probe was used. This probe sized droplets correctly, however, it failed intermittently. This introduced periods of missing data and ‘spikes’ during restarts. We removed the spurious data points and set the data to missing value if the total number of droplet counts was zero, assuming the SPP-100 had stopped recording data. During RF05, the SPP-100 failed and no data are available for this flight. In the case of RF03 and thereafter measurements of cloud droplets were also available from a Fast-FSSP (Brenguier et al. 1998). Intercomparison of the values of the total droplet number from the SPP-100 and FFSSP for the four flights for which this was possible show that the values of the FFSSP are within 20% of the values of the SPP-100, with the SPP-100 measuring higher total droplet concentrations for all flights.

As is generally known, the liquid water amount q_l derived from the SPP-100 is quite sensitive to the interpretation of calibration data. In the case of DYCOMS-II we found an average spread of 0.1 g m^{-3} by comparing left- and right-handed Riemann sums (as means of estimating the third moment q_l). Estimates of q_l using centered Riemann sums tended to underestimate q_l when compared to values as measured by bulk instruments like the PVM-100A (Gerber 1994) and the PMS-King probe. Compared to the PVM-100A the q_l values were 22% lower on average and compared to the PMS-King-probe 12% lower. However, in at least half of the cases the PVM-100A and King probe measurements were less than what would be implied by right-handed Riemann sums. Because the difference between the SPP-100 and the King and PVM-100A probes was on the order of the difference between the third moment of the distribution as calculated by right- and left-handed Riemann sums, we simply based our analysis on the center point of a bin and accepted the error implied by our inability to determine the size of a particle within a bin.

To determine the sizes of drizzle drops, one- and two-dimensional optical array probes were used. The one-dimensional Particle Measuring Systems 260X (260X) has a theoretical range in droplet diameter from 10 to 640 μm divided over 63 bins with an equal spacing of 10 μm; however, probe limitations combined with an aircraft speed of 100 ms^{-1} leads to a lower size limit of 40 μm in practice. Outside of a few periods in which the 260X was non-responsive, the probe functioned well during all flights. In particular, comparison (discussed below) with the two-dimensional optical array probe shows no discernible effect of the noise found to corrupt previous analyses (*e.g.*, Lasher-Trapp et al. (2002)). The two-dimensional optical array probe used for drizzle drops (2DC) detects particles with a diameter from 25 μm up to 800 μm distributed over 31 bins. The 2DC functioned properly with some exceptions; of these periods the whole of RF01 is the most noteworthy. In processing the 2DC data only particles which did not occlude either end diode were counted, this limits the size range of the probe but introduces fewer ambiguities.

The redundancy in instrumentation for the drizzle drops gives us the opportunity to compare the two. Plotting the first moment of the drizzle DSD (DDSD), as measured by both instruments, in one plot gives a first indication that in general the agreement between the two is quite good over a large part of the instrument's range. However, a more useful comparison is made when the fourth moment[†] is used as a proxy for the rainrate. Calculation based on 120s averages of the correlation and regression coefficients between 100 and 500 μm show that for flights RF02, RF03 (except the SF legs), RF07 and RF08 the correlation is high with values above 0.95. Together with best fit regression coefficients between 0.90 and 1.10 this indicates a good agreement between the 260X and the 2DC. For the SF legs of RF03 and flights RF04 and RF05 the agreement is poorer, with higher concentrations for the 260X than the 2D-C for the smaller drizzle drops.

Reflectivity data were obtained with the 95 GHz Wyoming Cloud Radar (Vali et al. 1998). The radar was operated with a dual antenna configuration but in this paper only data from the downward looking antenna is used. The analyzed reflectivity data had a vertical spatial resolution of 15 m (and sometimes 30 m) and a temporal resolution of one second. The radar was flown on every flight and almost continuous coverage exists with the exception of the SF legs which were too close to the surface to yield useful radar data. No attenuation corrections are applied to the data because the combination of shallow clouds with small liquid water contents yields attenuation values smaller than the 2dBz calibration accuracy. The noise level of the radar displayed little variation during DYCOMS-II so the data for all flights have been thresholded to exceed the noise level by one standard deviation based on an overall average of the recorded noise signal.

To compare the radar measurement of reflectivity Z_{radar} with the integrated reflectivity estimated from the *in situ* probes ($Z_{in\ situ}$), $Z_{in\ situ}$ has been estimated by integrating a lognormal distribution function fitted to 120s averages of the data (as will be explained in section 3.) and Z_{radar} is also averaged over 120s. As Figure 3 shows, the correspondence between the two estimates is fairly good. Exact agreement is not to be expected because the sampling volumes of the

[†] Drops in the drizzle drop range have fall speeds proportional to their diameter, (e.g., Rogers and Yau 1989) thus their mass flux is proportional to the fourth moment of the diameter

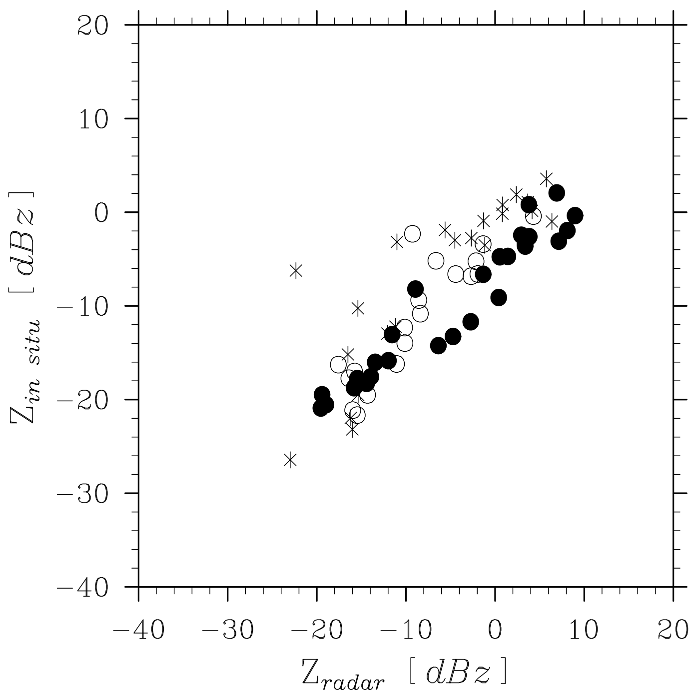

Figure 3: Comparison of reflectivity $Z_{in\,situ}$ and Z_{radar} with respect to RF02 for CT (closed circles), CB (open circles) and SC (asterisks) legs. $Z_{in\,situ}$ is calculated from the data from the SPP-100 and the 260X. The correlation coefficient with respect to the CB legs data points is 0.88 and the best fit regression coefficient is 0.82, indicating an acceptable agreement between $Z_{in\,situ}$ and Z_{radar} .

instruments differ by several orders of magnitude and are not coincident. The lack of coincidence arises because the radar during DYCOMS-II had a 140 m dead-zone so that the first radar return came from volumes $\sim$ 150 m below the flight level. Further, departures from the Rayleigh scattering regime at the tail of the DSD have not been accounted for. However, the error due to the expected height dependence of Z (increasing from cloud top to cloud base and decreasing from cloud base to the surface, see *e.g.*, Vali et al. (1998)) is evident in Figure 3: CT points tend to be to the right of the 1:1 line and SC points tend to be to the left, indicating lower and higher $Z_{in\,situ}$ than Z_{radar} values respectively. Because this error is most likely smallest for the CB legs, we calculated correlation coefficients (r) and best fit regression coefficients (s) for these legs. No coefficients were calculated for RF01 and RF05 because not enough data points were available to be statistically reliable. With $Z_{in\,situ}$ estimated from the SPP-100 and the 260X, r varied between 0.73 and 0.89 and s between 0.69 and 1.07. With regard to $Z_{in\,situ}$ estimated from the SPP-100 and the 2D-C, r varied between 0.82 and 0.97 and s between 0.70 and 1.11. Those numbers provide guidance when interpreting uncertainty but overall indicate a level of agreement which we find satisfactory.

3. Analysis methods

The *in situ* and remotely sensed data complement each other nicely. Computations of R from the *in situ* data are relatively unambiguous, but can be sensitive to errors in measurements of the larger drops, which can be poorly sampled, particularly given their low and variable concentrations. The better sampling statistics of the radar help to solve this latter problem and to the extent the ambiguity between the measured Z and the desired R can be resolved by the *in situ* data the radar can be used to quantify precipitation over a vertical plane as opposed to along a line defined by the trajectory of the aircraft. Although there are many objections to the use of generic Z-R relations, we minimize the inherent errors by using the *in situ* data to tailoring expressions valid on a flight to flight and level to level basis.

To do this we work entirely with *in situ* parametric representations of the *in situ* data. That is we fit functional forms to the *in situ* data and then estimate the relationship between R and Z implied by these functional forms. The motivation for working entirely with the *in situ* data is that it is self consistent, and as argued above, $Z_{in\ situ}$ is consistent with Z_{radar} , moreover Z_{radar} data was not available for the surface legs. The motivation for fitting the data is that it reduces the amount of data one has to work with to a manageable level, with no apparent loss in vital information, and it provides a framework for estimating uncertainties. Further, to the extent one is confident in the fits, fitting can supply us with some extra information by extrapolating the fit to drop diameters beyond the measurement range of the instrument.

a. Distribution fitting

The choice for a specific fitting function is to a certain extent an arbitrary one and although other distributions (such as the gamma function) also are attractive, we have chosen to use the lognormal one, partly because the lognormal function has been applied successfully in the past (*e.g.*, Feingold and Levin (1986) and references herein, and Gerber (1996)) and partly because we were most familiar with it. Another attractive feature of the lognormal distribution is that it is the expected distribution for a drizzle spectrum which is produced through a coalescence process dominated by log-range (in diameter or mass space) interactions (Aldous 1999). The lognormal distribution function is given by:

$$N(D) = \frac{N_0}{D\sqrt{2\pi ln^2\sigma_g}} e^{\frac{-(lnD-\overline{lnD})^2}{2ln^2\sigma_g}}, \tag{1}$$

with $N(D)$ the number of drops per size interval, N_0 the total number of drops, $ln^2\sigma_g = \overline{(lnD-\overline{lnD})^2}$ and D the diameter. Advantages of a lognormal distribution are that higher powers of a DSD are lognormally distributed as well and that distribution parameters have physical meaning: D_g is the geometrical mean diameter or median of the size distribution given by:

$$D_g = e^{\overline{lnD}}, \tag{2}$$

and σ_g represents the geometric standard deviation or width of the distribution. Thus the fitting parameters act as proxies for the behavior of the DSD's in time and space, thereby effecting a considerable reduction in the data.

We fitted truncated lognormal functions to the observed DSD's (following Feingold and Levin (1986)). This constrains the fitted distribution to have the same moments as the observed distribution over the measured size range. We fitted two lognormal distributions: one to the CDSD and the other to the DDSD. Figure 4 illustrates that this makes sense because two distinct modes are evident in the DSD. The lognormal distribution functions are fitted to DSD's averaged over two minutes (equivalent to roughly 12 km). The choice for an averaging period of two minutes is dictated by the DDSD and is a trade off between a longer period which would reduce the sampling error and a shorter period which would allow more details to be kept in the spatial and temporal scales (see also Appendix A).

In order to derive the uncertainties in the fitting parameters, an uncertainty in the DSD's has to be estimated. Because the exact instrumental error in the measurements is difficult to establish, we have chosen to take the variance in the DSD as such. A disadvantage of this is that the variance contains a large contribution (especially with respect to the larger drizzle drops) due to under sampling by the instruments. In order to overcome this drawback we reduce the output frequency of the *in situ* instruments by applying an intermediate averaging period of 20 seconds and define the standard deviation in the 2 minute averaged DSD as the square root of the variance in those six intermediate DSD's (for more information see Appendix A). Once the fit is determined, the uncertainties in the fitting parameters are calculated by first computing the χ^2 value of the fit and next by determining how much the fitting parameters (one at a time) have to be varied in order to raise the χ^2 value around its local minimum by 1. (Bevington and Robinson 1992). For more information see Appendix A.

Before integrating the lognormal distributions to calculate R and Z we need to specify integration limits. For the CDSD the lower limit and upper limit of the size range of the SPP-100 are taken as D_{min} and D_{max} respectively. For the DDSD D_{min} is taken equal to D_{max} of the CDSD in order to avoid either an overlap or a gap between the two distributions. For the standard calculations we chose to extrapolate the lognormal fit to D_{max} = 1 mm. In section 5. sensitivity studies are presented to show the sensitivity of the choice for D_{max}. More technical details about the fitting can be found in Appendix A.

In Figure 5 an illustration of the fitting parameters acting as proxies for the behavior of the total DSD's is provided. In Figure 5 (panel a) two CDSD's measured by the SPP-100 and two DDSD's measured by the 260X are shown, both are two minute averages from the first CT leg from RF07. One shows DSD's during a period of heavy drizzle while the other is representative of a period with light drizzle (rain rates four times as low). If we compare the DSD's we see that during the period of heavy drizzle the CDSD has a broader distribution, with a larger mean diameter and fewer droplets. The heavy drizzle DDSD shows a higher count of drops and a slightly larger mean diameter. Whether or not there is a difference in broadness is hard to judge by eye. The same information can be obtained, but much faster, from Panels b, c and d which show the evolution of N, D_g and σ_g along the flight leg, both for the SPP-100 and the 260X. The two DSD's shown in 5a are the ones at 23 min and 29 min respectively, with the one at t = 23 min being the heavy drizzle one.

With help of the lognormal distribution functions we analytically calculated two values for the *in situ* drizzle rate: one based on a combination of the 260X-SPP-100 data set and one based on a

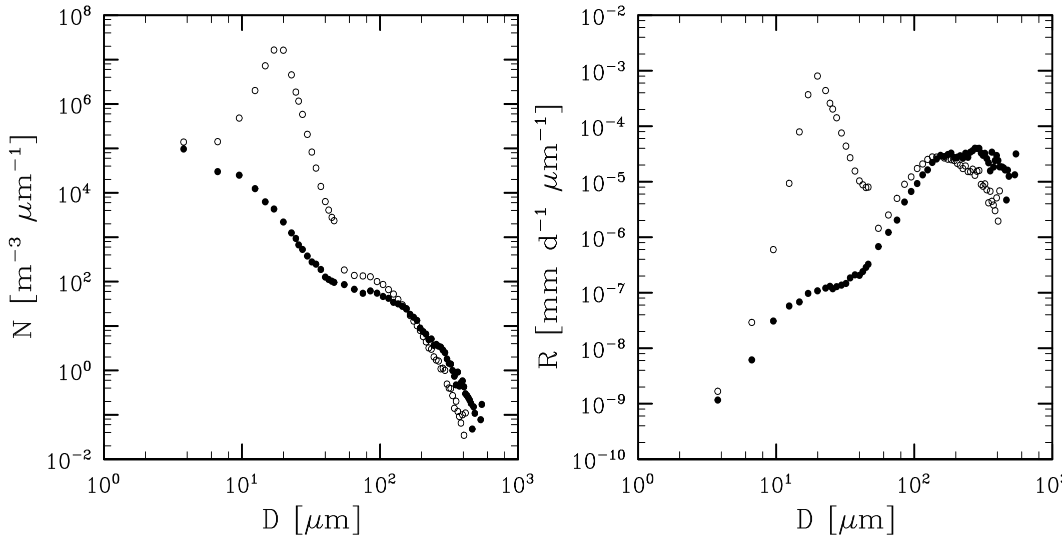

Figure 4: Leg averaged drop concentration N and drizzle rate R as function of the drop diameter D with regard to the second CT leg (closed circles) and first SC leg (open circles) of RF07.

combination of the 2D-C-SPP-100 data set. A comparison between the two shows good agreement. Half of all the values of the drizzle rate based on the 260X combination are within one sigma of the drizzle rate based on the 2D-C combination and 90% of the data points are within two sigma. The differences between the two drizzle rates are mainly due to (small) differences in the right tail end of the lognormal fits which magnify due to our choice of extrapolating the fits up to 1 mm. When the calculations are done up to 500 μm instead, the numbers rise to around 80% and almost 100% respectively. In the rest of the article we have chosen for the sake of brevity to present *in situ* values for R (denoted by $R_{in\ situ}$) and Z (denoted by $Z_{in\ situ}$) based on data of the 260X and the SPP-100 only. First of all because we consider the 260X data to be slightly more reliable and secondly because the 2DC data had not enough acceptable 2 minute fits for the SF legs to ensure a reliable R-Z relationship needed for the radar reflectivity conversion into drizzle rate (see section below)

Because a reduced description of the DSD as collected across DYCOMS-II flights may be broadly useful, and facilitate subsequent investigations some of which may want to check our work, we have collected our fitting parameters into files which are available from the DYCOMS-II archive.

b. Z-R relationships

An example of the rainrate reflectivity relationships that emerge from the fitted distributions during RF02 is shown in Figure 6. This figure demonstrates the extent to which a power-law relation between R and Z is supported by the data, it also shows that there is merit in performing the analysis at different levels. The tendency of R to vary less sharply with Z in the cloud is consistent with the physical expectation of the precipitation flux being carried by smaller particles (whose fall velocity

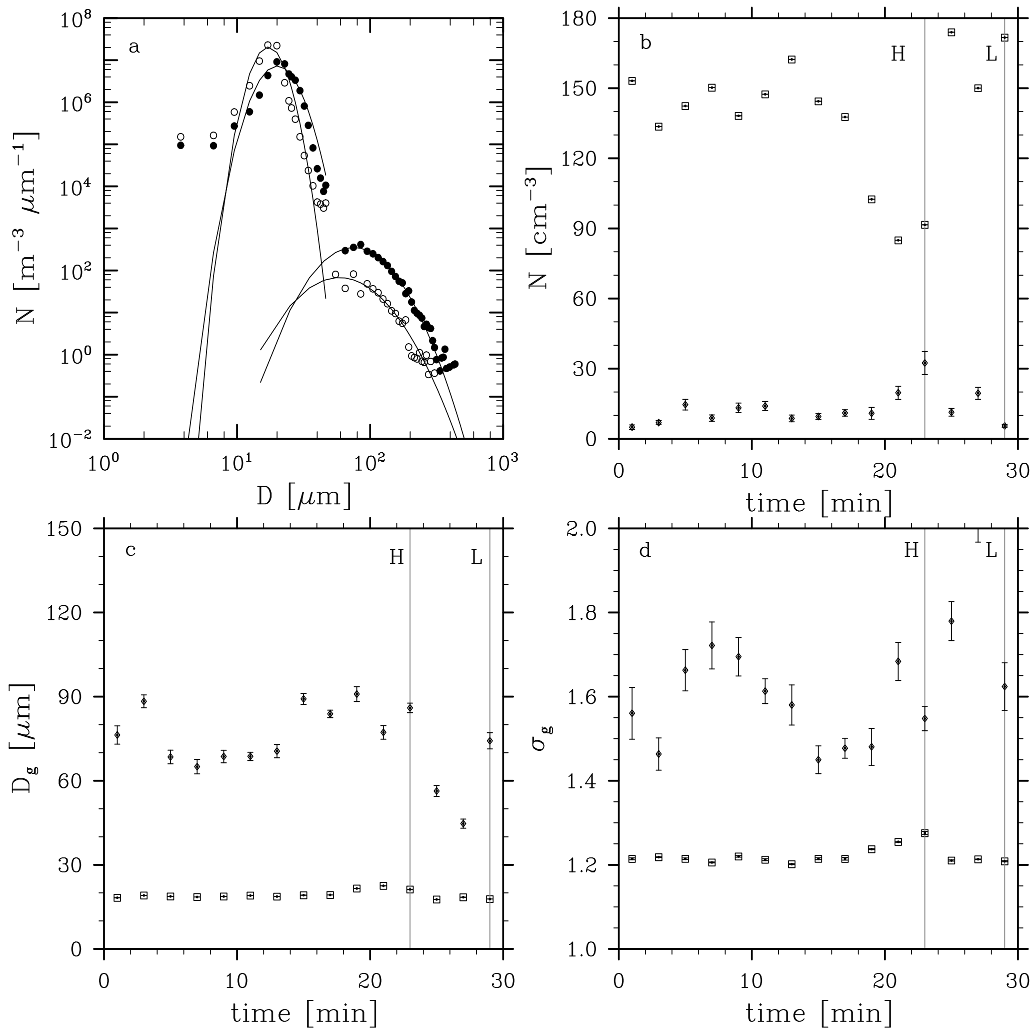

Figure 5: Data from the first CT leg of RF07. a) DSD of one 2 min period with heavy drizzle (closed circles) and one 2 min period with light drizzle (open circles). For both the 260X (closed diamonds) and the SPP-100 (open squares) b) drop number N (note for the 260X, N is multiplied by 1000) c) geometrical mean diameter D_g and d) geometrical standard deviation σ_g as function of time. The H denotes the 2 min period of heavy drizzle and the L the period of light drizzle.

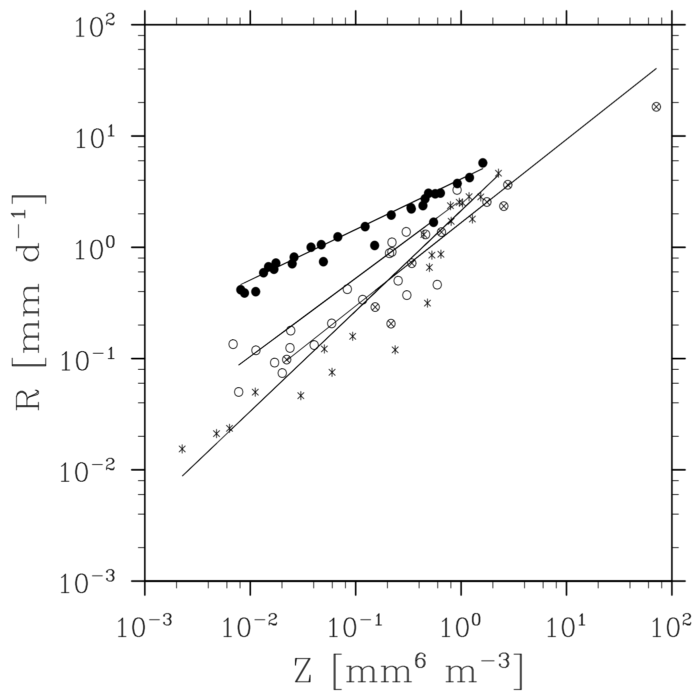

Figure 6: Drizzle rate $R_{in\ situ}$ versus reflectivity $Z_{in\ situ}$ for RF02 at four different leg heights: CT (closed circles), CB (open circles), SC (asterisks) and SF (encircled crosses). Best fits are also given based on the two legs flown at each height.

is proportional to D^2) near cloud top and larger particles (whose fall velocity is proportional to D) lower down. Although above we show $R - Z$ relations for each flight and for each flight level, in the remainder of the manuscript we focus on two levels: one corresponding to the height of the SF legs, which we call the surface, and one at the height of the CB legs, which we call cloud base.

More generally, in Table 2 we present $R - Z$ relations valid at cloud base and at the surface for each flight for which significant drizzle was evident. The uncertainties in these relations are estimated by propagating the uncertainties in our fits of the distributions. The relationships in Table 2 will be used in section 4.. To avoid ambiguity with *in situ* drizzle rates, those calculated from the radar reflectivity will be denoted by R_{radar} .

4. Variability of drizzle

Keeping in mind that an R of 1 mm d^{-1} is roughly equivalent to a heat flux of 30 Wm^{-2} (which is in general comparable to half the net long-wave radiative flux divergence at cloud top), the flight averaged drizzle rate $\langle R \rangle$ in Table 1 gives a first impression of the importance of drizzle for the overall energetics of the PBL. Based on this, the seven flights naturally divide into three groups. RF02 and RF07 can be characterized as 'heavy' drizzle cases, while in flights 3, 4 and 8 only a modest amount of drizzle reached the surface. Both RF01 and RF05 belong to the 'very light'

flight	a	n	a	n
level	SF		CB	
RF02	1.66 ± 0.27	0.75 ± 0.13	2.66 ± 0.25	0.70 ± 0.04
RF03	0.94 ± 0.38	0.62 ± 0.15	1.82 ± 0.19	0.61 ± 0.03
RF04	0.86 ± 0.49	0.58 ± 0.18	1.66 ± 0.12	0.59 ± 0.04
RF07	1.12 ± 0.23	0.66 ± 0.13	2.13 ± 0.10	0.68 ± 0.04
RF08	1.22 ± 0.24	0.47 ± 0.04	2.68 ± 0.10	0.46 ± 0.01
'night'	1.31 ± 0.14	0.74 ± 0.04	2.03 ± 0.07	0.64 ± 0.01
'all'	0.51 ± 0.03	0.34 ± 0.02	2.27 ± 0.06	0.48 ± 0.01

Table 2: Values for parameter a and power n in the R-Z relationship $R = aZ^n$ based upon the data of the SPP-100 and 260X, both of the SF legs and the CB legs. For RF01 and RF05 not enough data points are available from the *in situ* data so in these cases R was related to Z using a relationship derived from the average of either all the nocturnal flights, or all of the flights.

or 'no drizzle' group because only trace amounts of drizzle reached the surface. Incidentally a qualitative analysis of radar echoes from RF06 and RF09 whose flight pattern were not conducive to the type of analysis we wished to conduct put them in the 'heavy' and 'very light drizzle' categories respectively.

The flights during DYCOMS-II support the common view of an existing diurnal cycle in the drizzle rate (*i.e.*, higher drizzle rates during the night compared to lower daytime values), especially if RF06 (nighttime flight) and RF09 (daytime flight) are taken into account as well. However, the experimental strategy did not allow us to detect an early morning maximum in the drizzle rate (Kraus 1963).

In the analyses we define drizzle as having a drizzle rate of at least 0.03 mm d^{-1} to avoid different minimum R_{radar} thresholds for every leg. (Note that this lower limit is equivalent to the removal of one liter water per day over an area of 5 by 6 m.) Hereafter, we will refer to drizzle rates of 1 mm d^{-1} and higher as heavy drizzle.

a. Interflight variability

While most physically based investigations have rightfully focused their attention on physical interactions, less attention has been devoted to the question of the statistics of drizzle as a function of cloud macroscopic properties. It seems worthwhile to take a more empirical approach and ask whether in spite of such complexities observed drizzle rates co-vary in some simple way with cloud macrophysical properties. Such an approach is motivated by the realization that many simple microphysical models produce such scaling in their stationary limit (*e.g.*, Pincus and Baker (1994)), and recent observational work which suggests that the cloud averaged drizzle flux scales with H^4/N, where H is the cloud depth and N denotes the cloud droplet concentrations in adiabatic regions of the cloud layer (Pawlowska and Brenguier (2003)). In addition to providing a target for future theoretical work, such relationships (insofar as they exist) can form the basis for parameterizations of drizzle in large-scale models, and also aid retrievals of drizzle from satellite

flight	H [m]	N [cm^{-3}]	Δ_T [K]	$R_{radar,cb}$ [mm d^{-1}]
RF01	265	140	n/a	0.05
RF02	360	58	1.6	1.24 $\pm$ 0.17
RF03	390	254	3.3	0.18 $\pm$ 0.02
RF04	465	205	2.2	0.76 $\pm$ 0.07
RF05	275	151	3.1	0.04
RF07	515	135	1.9	1.65 $\pm$ 0.13
RF08	330	113	2.3	0.38 $\pm$ 0.02

Table 3: Macroscopic variations in cloud structure and rainrates among flights. See text for definitions.

derived estimates of cloud macroscopic properties.

To begin, we follow the lead of Pawlowska and Brenguier (2003) and ask to what extent the drizzle rate at cloud base scales with H and N. In this analysis we estimate H using the data tabulated in Stevens et al. (2003a), which corresponds to the difference between the flight averaged cloud top height, $\langle h_{ct} \rangle$, and the flight averaged cloud base height, $\langle h_{cb} \rangle$. The former is derived from lidar measurements of cloud top made during the three RL legs (roughly 90 minutes of 1 s^{-1} data). The latter is based on roughly four hours (per flight) of *in situ* data collected from flight legs flown in or below the cloud layer. Variability in h_{ct} and h_{cb} was typically 20-50 m, although in RF04 and to a lesser extent in RF05 there is evidence of an almost discreet change in cloud top and base indicative of sampling across two distinct air-masses. To estimate N we average the SPP-100 data from all the cloud legs, which typically corresponds to two hours of data. Because N tends to vary relatively little through the depth of the cloud, such an average seems warranted. For the radar derived drizzle rate at flight averaged cloud base $R_{radar,cb}$ we use reflectivity the time-series from the CT and RL legs, which corresponds to, on average, 150 min of data per flight.

Values of H, N and $R_{radar,cb}$ calculated in the above described manner are given in Table. 3. As illustrated in Figure 7 these data seem to support an $R_{radar,cb} \propto H^3/N$ relationship. This finding differs slightly from the H^4/N scaling for R_{cloud} that Pawlowska and Brenguier found for clouds sampled during the second Aerosol Characterization Experiment (ACE-2).

Past studies have also attempted to relate drizzle to satellite based estimates of particle size, such as the cloud-top effective radius r_e. For instance, using ground and satellite based remote sensing Han et al. (1995) argue that drizzle could be associated with occurrences of satellite derived estimates of $r_e > 15\mu$m, and that clouds could be categorized as non precipitating when $r_e < 10\mu$m. Using only *in situ* data Gerber (1996) presents evidence that whenever r_e exceeds a 16 μm threshold, drizzle tends to be heavy. He argues that this suggests the presence of a coalescence threshold, (*e.g.*, Hocking (1959)). Shiptrack data analyzed by Ferek et al. (2000) also show evidence of a threshold-like dependence of drizzle on cloud-top effective radius, with a threshold lying somewhere between 9 and 14 μm. Note that the somewhat more fuzzy threshold behavior in the Han *et al.*, and Ferek *et al.*, studies relative to the measurements of Gerber may in part be due to the different nature of the sampling. Gerber's measurements essentially show a discreet change in

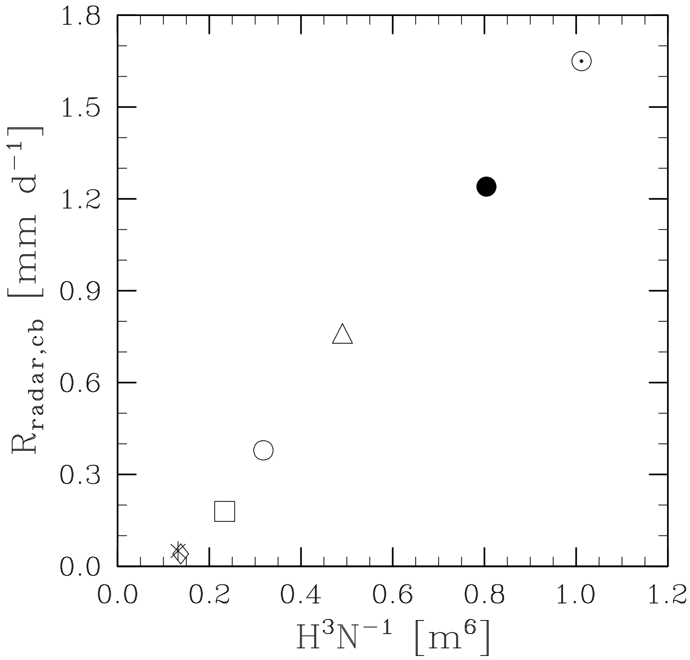

Figure 7: Cloud base drizzle rate, $R_{radar,cb}$, as a function of cloud depth cubed, H^3, divided by the total cloud drop number N. Each flight is denoted by a specific marker: RF01 asterisks, RF02 closed circle, RF03 open square , RF04 open triangle, RF05 diamond RF07 open circle with dot, RF08 open circle.

the structure of the local droplet spectrum as its effective radius increases beyond a certain value. The other studies speak more to the aggregate properties of precipitating versus non precipitating cloud layers. For the purposes of this study we are more interested in the latter.

To address the question of a possible relationship between the drizzle rate and r_e we compare $R_{radar,cb}$ with r_e estimated using *in situ* data collected along the cloud top legs. For these purposes we estimated r_e from the fits to the SPP-100 and 260X data. Results from all the analyzed flights are plotted in Figure 8. Overall they support the idea of threshold-like behavior between 10 and 15 μm. However the transition between large and small values of $R_{radar,cb}$ is not particularly sharp and there is evidence of systematic differences among flights. Because for an adiabatic cloud r_e scales with $H^{1/3}$, this is not likely to be due to systematic differences in relative distance from cloud top among flights (and hence biases in our estimate of r_e). It is, however, consistent with the fact that if $Nr_e^3 \propto H$, to the extent that $R_{radar,cb} \propto H^3/N$ holds on the 12 km scale, one would expect $R_{radar,cb}$ to depend on both r_e and N according to $R_{radar,cb} \propto r_e^9 N^2$.

Finally we compare drizzle rates to the difference Δ_T between the 11 and 4 μm brightness temperatures as measured by GOES-10. This is instructive because the comparison between the drizzle rate and r_e as derived from satellite are made more difficult by the lack of standard nocturnal retrievals for r_e, and the tendency of the daytime retrievals to fail in regions where the cloud become more broken. Because drizzle seems to correlate with more broken clouds (see Figure 1)

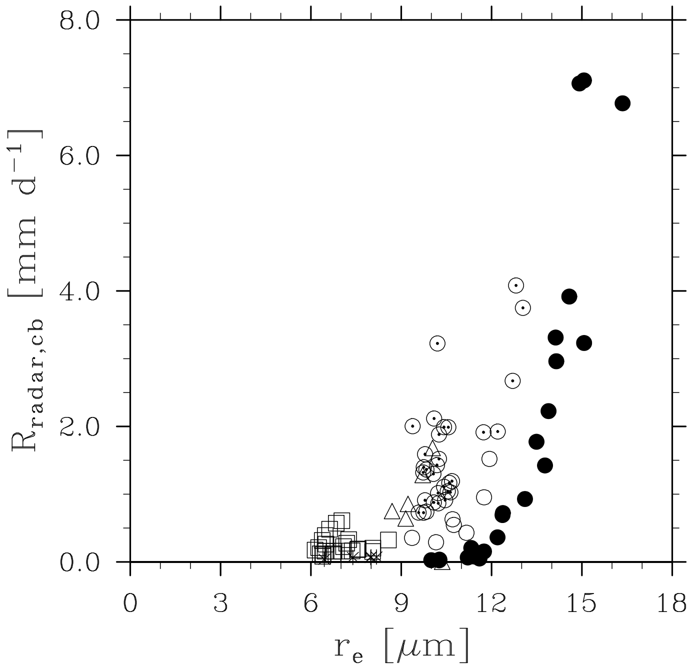

Figure 8: Cloud base drizzle rate, $R_{radar,cb}$, versus the effective radius r_e at cloud top for all flights except RF05. Symbol follow the convention of Figure 7, with each data point representing two minutes of data.

such a failure might significantly bias the measurements. Using Δ_T instead is feasible because *e.g.*, for a cloud with an optical depth of 15, changes in r_e from 6-12 μm will result in a decrease of Δ_T from approximately 5 K, to nearly 1 K. In contrast, such changes at a fixed value of r_e would require a 15 fold reduction in the optical depth (*cf.*, Figure 1 of Perez et al. 2000). All flights except RF08 were nocturnal, so Δ_T values were estimated using the 1200 UTC GOES-10 image, while for RF08 the 0300 UTC image was used. Using Δ_T^{-1} as a proxy for drop size, Table 3 shows a clear tendency for bigger drops to be associated with fewer drops and more drizzle. RF06 and RF09, whose flight patterns were not conducive to the quantification of drizzle, also fit this pattern. By using $0.25K < \Delta_t < 2K$ as a proxy for regions where $R > 1$ mmd^{-1} then the nightime imagery can be exploited to estimate drizzle rates over larger areas. In the 1200 UTC GOES nighttime imagery, the box bounded by 35S, 30S, 125W and 120W has $R > 1$ mmd^{-1} in overcast regions 27% of the time. This proportion of drizzle is consistent with the fact that approximately one third of the DYCOMS flights measured significant to heavy drizzle at cloud base.

b. Horizontal variability

Figure 9 and 10 show the spatial distribution of drizzle for flights RF02 and RF07, the two nighttime flights with the highest $\langle R\rangle$. The precipitation rate at flight level can be read by subtracting the baseline height and associating 100 m increments with 1 mm d^{-1}. For both flights we show

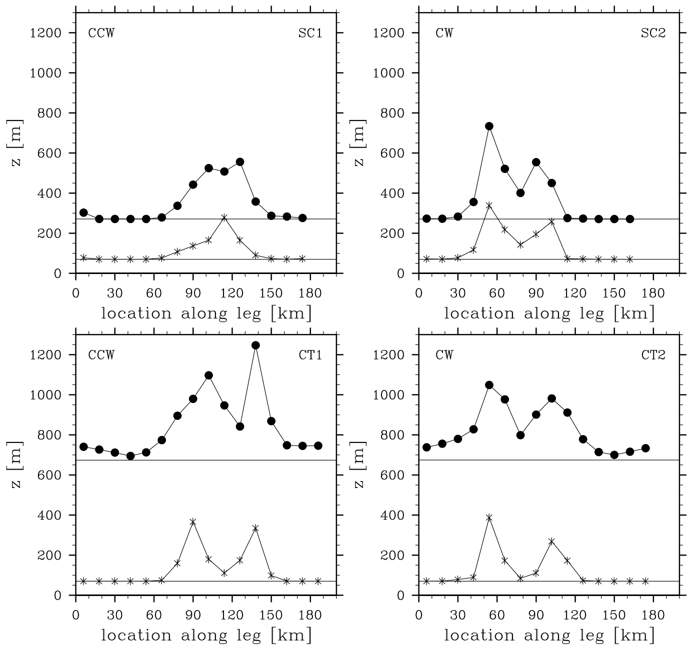

Figure 9: Drizzle rate R during RF02 for the two SC and CT legs as function of location along the flight leg. Here $R_{in\ situ}$ (closed circles) and R_{radar} (asterisks) are plotted relative to a baseline denoting the measurement level, with 1 mm d^{-1} corresponding to 100m. The flight direction (counterclockwise (CCW) and clockwise (CW)) is specified in the upper left corner of each panel.

data from the two SC and CT legs since they form a representative cross section of the whole flight and were flown consecutively (except for the case of RF07 where the CT legs were interrupted by the remote sensing leg whose radar echos shown in Figure 2).

It is reassuring to see the similarity in spatial structure (on the order of ten km scale) between the *in situ* data and surface radar data. To a certain extent this is expected but on the other hand several factors could have contributed to differences between the two. Drizzle measured at a cloud base of 500 m could be expected to reach the surface nearly 30 min later (*i.e.*, assuming a mode diameter of 100 μm which corresponds to a fall speed of 0.3 cm s^{-1}), hence if the timescale of drizzle evolution is much shorter than this we would anticipate little coherence in the vertical. The degree of vertical coherence observed is consistent with the apparent temporal coherence, as evident in the persistence of the envelope of precipitation among two or even more legs. (Keep in mind that consecutive legs are flown in opposite direction, thus R in the different panels displays a mirror symmetry.) Other indications of a time scale for drizzling regions of at least an hour and potentially much longer can be found when radar echo images of consecutive legs are studied by eye: a clear persistence on larger scales is quite often visible.

An apparent difference between RF02 and RF07 is the higher background drizzle rate of RF07. The large-rain rates observed during RF02 appear to be localized into small regions or cells. The contribution of such cells to the overall drizzle rate of RF07 seems less pronounced. The net contribution of regions of varying precipitation rate to the observed accumulation is perhaps better

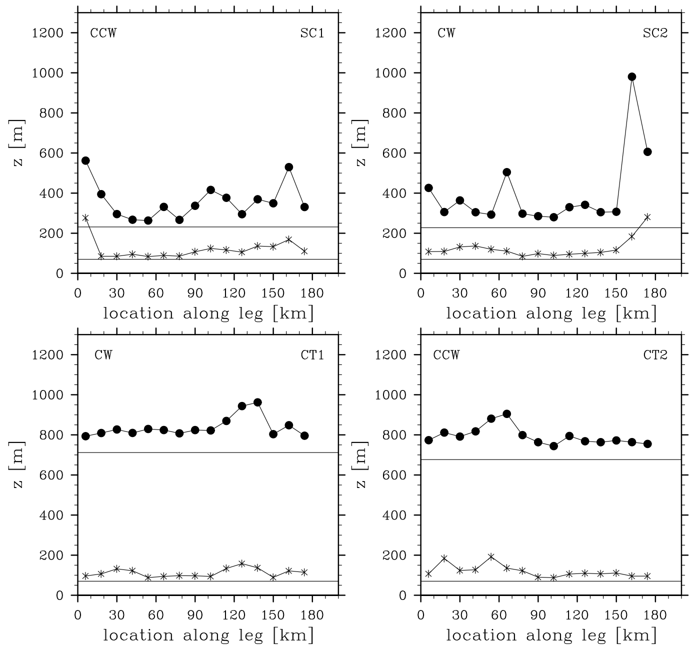

Figure 10: As in Fig 9, but for RF07

illustrated in Figure 11. Panel a of this figure presents normalized distributions of R_{radar} for RF02, RF07 and RF04; RF03 and RF08 behave similar to RF04 and are left out for clarity. The drizzle rate on the vertical axis denotes the amount of drizzle in the bin interval as a fraction of $\langle R \rangle$ (Table 1). Note that the bins on the horizontal axis are logarithmic. Panel b shows the cumulative distribution of R_{radar} scaled with $\langle R \rangle$ as function of the fraction of the total drizzling area. The percentage of the total flight path length with drizzle at the surface can be obtained from Table 4. The straight line depicts a uniform distribution.

The visual similarity among the three distributions in Figure 11a is supported by a more quantitative analysis, suggesting that the distribution of drizzle intensity could be captured by a simple parametric representation. However because of the logarithmic abscissa, a rightward shift of the distribution sharply increases the extent to which the relatively rare, but intense drizzle events contribute to the overall distribution. This is evident in Figure 11b which shows that in the case of RF02 only 20% of the drizzling area is responsible for 80% of the total amount of drizzle removed from the boundary layer. Further insight into these issues is provided in Table 4 which examines how frequently drizzle reaches the surface on a given flight, and what fraction of the drizzle can be considered heavy. Besides showing once more the importance of the heavy drizzling cores to the overall drizzle rate the Table also shows that low overall drizzle rates correlate with a low intensity of drizzle. Interestingly this implies that the greater the value of $\langle R \rangle$ the more likely it is that drizzle (of a significant amount) covers small spatial areas—which is consistent with the idea that drizzle could induce a transition in cloud structure (Stevens et al. (1998) and Paluch and Lenschow (1991)).

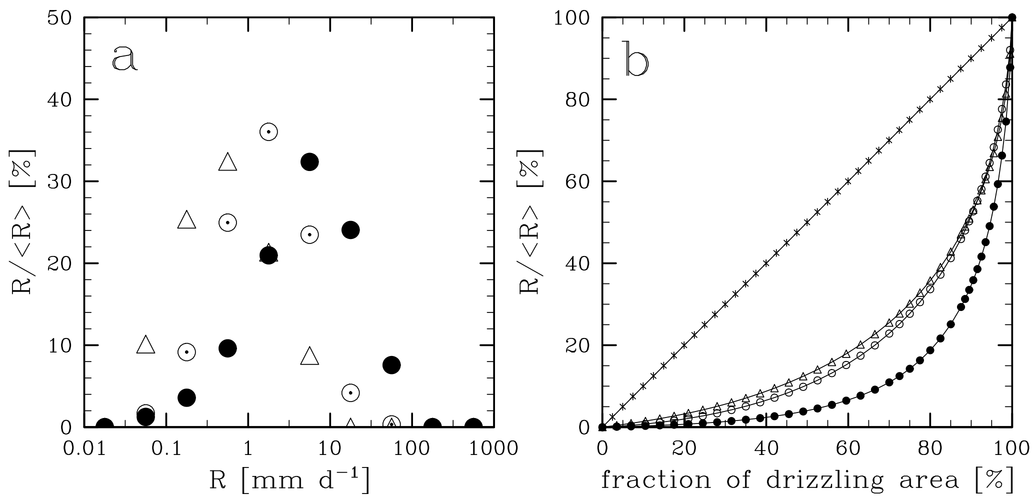

Figure 11: a) Distribution of the drizzle rate intensity for RF02, RF07 and RF04 as function of the relative contribution to $\langle R\rangle$ and b) the cumulative distribution of R scaled with $\langle R\rangle$ as function of the fraction of the total drizzling area. Symbol representation similar to Figure 7.

c. Dependence on droplet spectra

Even though it is to be expected from first principles, and clearly supported by Figure 7, measurements are not available to examine the influence of local cloud depth on local drizzle rates. Although cloud top can be detected when flying above the cloud and looking down, the radar does not well represent cloud base. Similarly, when flying below the cloud the local lifting-condensation-level can be used as a proxy for cloud base, but in this case no cloud top information is available. On the other hand, we can gain some insight by examining the correlations between$\langle R\rangle$ and the parameters of the fitted droplet distributions. Figure 12 shows that the best correlation is found between the number of drizzle drops and $R_{in\,situ}$. This indicates that increased drizzle is not accompanied by a change in shape of the part of the droplet distribution associated with drizzle. This suggests that it might suffice to model the drizzle mode using a one parameter distribution. There is also evidence of a weaker negative correlation between $R_{in\,situ}$ and the number of cloud droplets. Together with a constant D_g, both for the cloud and the drizzle drops, and a slight broadening of the CDSD, this is consistent with the scavenging of cloud droplets by precipitation. For another example see Figure 5b. Signs of precipitation scavenging were also noticed by Austin et al. (1995); *e.g.*, their Figure 7.

Using the fact that D_g and σ_g appear to be (nearly) constant over a leg, we estimate how much of the variability in $R_{in\,situ}$ can be associated with variability in N. To do this in Figure 12a we compare R_N with $R_{in\,situ}$, where R_N is the value $R_{in\,situ}$ would have if D_g and σ_g were fixed at their mean values. R_N captures the variability of R very well and no systematic bias is evident. This is also demonstrated by the fact that $\overline{R}$ and $\overline{R_N}$ (with the over-bar denoting leg averaged values) are so close that the two lines indicating those values in the figure are indistinguishable.

Figure 13 reveals that similar results are valid for other legs as well. The figure presents $\overline{R}$

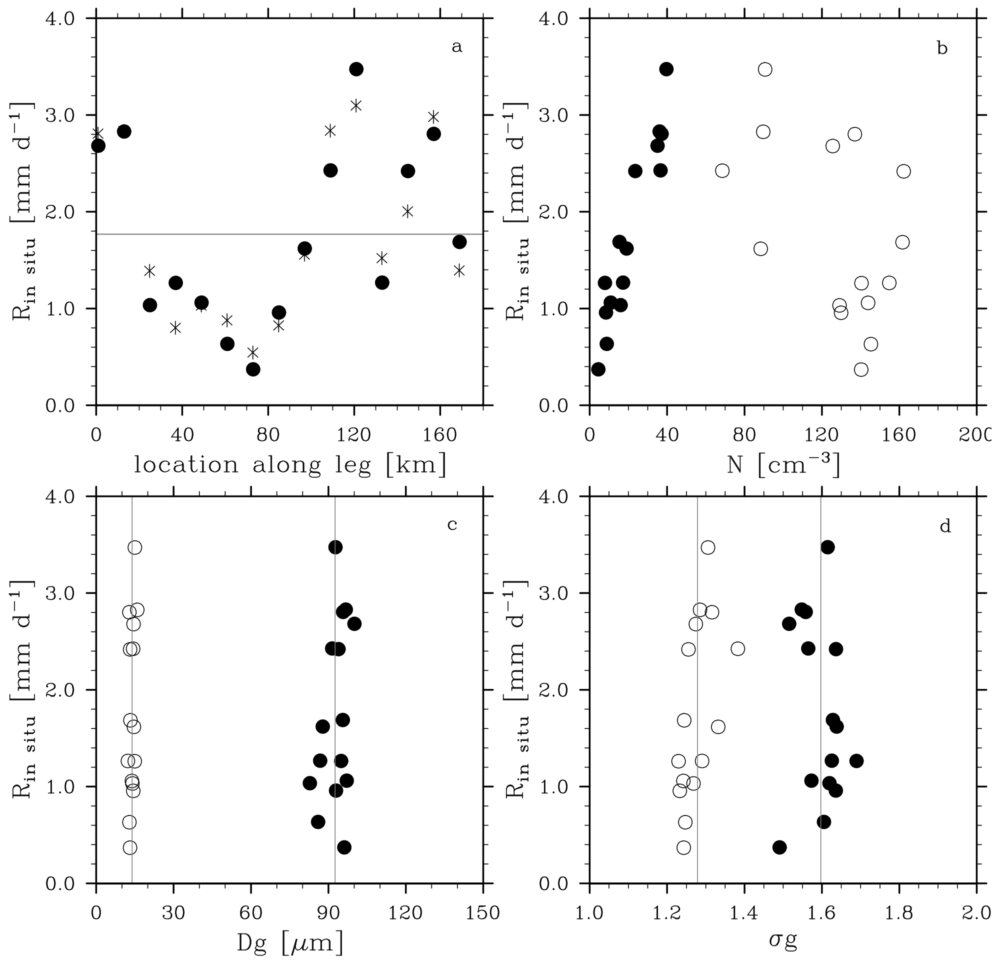

Figure 12: Correlation between the *in situ* drizzle rate $R_{in\ situ}$ and the fitting parameters for the first cloud base leg of RF07. a) Drizzle rate $R_{in\ situ}$ in time (closed circles) and drizzle rate R_N (asterisks) calculated as function of droplet concentration N and the leg averaged values of the geometric mean D_g and the geometric standard deviation σ_g. The thin lines denote the leg averaged value of both drizzle rates; because they are nearly identical for this leg the lines lie on top of each other. b) $R_{in\ situ}$ versus N (note that the drizzle drop number is multiplied with a factor 1000 in order to fit both drop numbers in one plot), c) $R_{in\ situ}$ versus D_g and d) $R_{in\ situ}$ versus σ_g. The data points based on the 260X are denoted by the closed circles; those based on the SPP-100 by the open circles. The leg averaged values of D_g and σ_g used in the calculation of R_N are shown by the thin lines in c) and d).

flight	L_R/L_{tot} [%]	L_{Rcore}/L_{tot} [%]	R_{core}/R_{tot} [%]
RF01	0.1	0.0	0.0
RF02	27.0	6.6	85.4
RF03	27.7	0.6	19.7
RF04	31.1	1.2	30.6
RF05	0.0	0.0	0.0
RF07	85.6	15.8	64.1
RF08	44.1	1.9	23.7

Table 4: Values for each flight of the percentage of time or space that drizzle is detected at 70 m above the sea surface, that heavy drizzle ($R > 1$ mmd^{-1}) is detected and the contributions of heavy drizzle to the total drizzle rate

versus $\overline{R_N}$ for all seven flights. The correlation between the two is high with r of 0.95 and the data does not deviate a lot from a one-to-one line. Comparison of $\overline{R}$ with $\overline{R_{D_g}}$ and $\overline{R_{\sigma_g}}$ (calculated with local values of D_g and σ_g respectively and leg averaged values of the other two fitting parameters) displays more scatter and lower correlation coefficients, albeit still with acceptable values. With respect to $\overline{R}$ and $\overline{R_{D_g}}$, r has a value of 0.73 and for $\overline{R}$ and $\overline{R_{\sigma_g}}$ r is 0.78. An interesting side effect of R_N explaining most of the variability in $R_{in\ situ}$ is the fact that a drizzle rate calculated with leg averaged values for all three fitting parameters (thus representing a leg averaged R_N) has the same high r of 0.95, due to the fact that the calculation of the drizzle rate is linear in N.

d. Subcloud evaporation

To investigate evaporation in the subcloud layer we calculate the fraction of the cloud base drizzle rate which reaches at the surface, and plot this versus the depth of the subcloud layer in Figure 14. Here our analysis is limited to time periods when we have simultaneous estimates of $R_{radar,cb}$ and $R_{radar,sfc}$. Even for rather shallow subcloud layers most of the precipitation evaporates before reaching the surface. Despite the spatial inhomogeneity of drizzle the leg averaged evaporation values are fairly constant for each flight and display only a slight dependence on the subcloud layer depth. The relatively less evaporation which occurs in some legs of RF02 (and to a lesser extent RF07 as well) may reflect the influence of humidified cores, *i.e.*, the correlation between sub-segments of the leg with increased precipitation and increased humidity in the subcloud layer.

5. Discussion

It might seem perplexing that in section 4c. we show that R scales with N, yet in the Z-R relationship scales as $Z^{2/3}$. For a lognormal distribution, one would expect that if variations in R are explained by variations in N, then R should scale with Z, rather than with $Z^{2/3}$ (e.g., Feingold and Levin (1986)). For two reasons, this is not as contradictory as it seems. First, the other parameters

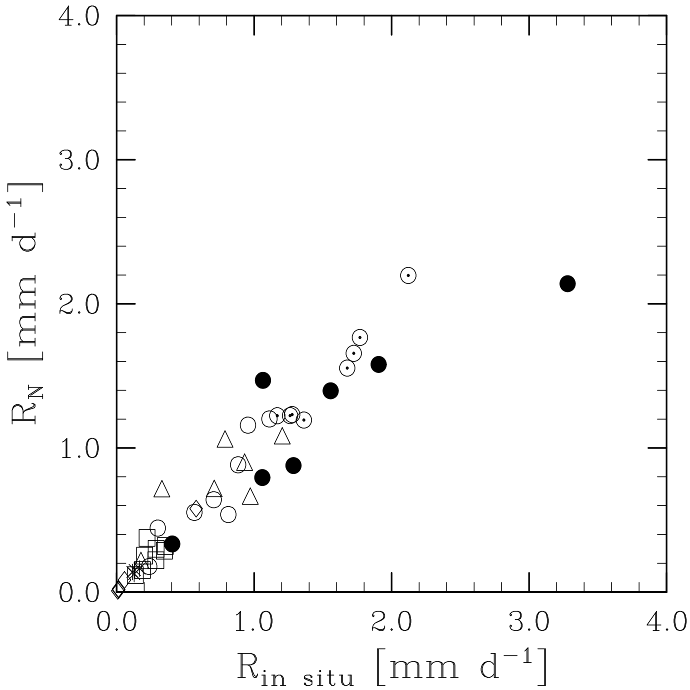

Figure 13: Leg averaged values of drizzle rate $R_{in\,situ}$ versus drizzle rate R_N (see Figure 12 for definition) for each flight. Symbol representation identical to Figure 7..

in the lognormal distribution, *i.e.*, D_g and σ_g, are not independent of N, as the simple argument which leads to the $R \propto Z$ scaling requires. Additionally, the tendency of R to scale with $Z^{2/3}$ is based on log-space regressions, which weight points irrespective of their contribution to the net drizzle rate, i.e., points which contribute negligibly count as much as points which weight more. The finding that N variation explain most of the variability in R is based on relations in linear space, which discount points whose contribution to the net R are negligible.

These differences highlight just some of the difficulties in the R-Z relationships which form the basis for the underlying precision of our analysis. Although we have tried to bound any uncertainty by a careful consideration of errors, it is also useful to investigate how sensitive our results are to some of the underlying assumptions, such as our decision to use extrapolated log-normals, or our belief that it was best to tailor R-Z relations on a flight by flight basis. To answer these questions we provide estimates of surface rainrates among flights using two alternative methods of analysis: no extrapolation of the lognormal functions and a generic R-Z relationship for DYCOMS-II.

The 'no-extrapolation' relationship was computed by determining the maximum diameter present in the measured DSD (with respect to every two minute average) and using this value as upper limit in our calculation of respective $R_{in\,situ}$ and $Z_{in\,situ}$. In Table 5 we present the flight averaged surface drizzle rates computed with the this R-Z relationship. The $\langle R \rangle$ values are higher than in Table 1 (all within one standard deviation, except RF07), with the largest increases going with the larger drizzle rates. The reason for this is that truncation of the spectra leads to higher values of both the slope (n) and pre-factor (a) of the $R - Z$ relationship. With respect to $Z_{in\,situ}$

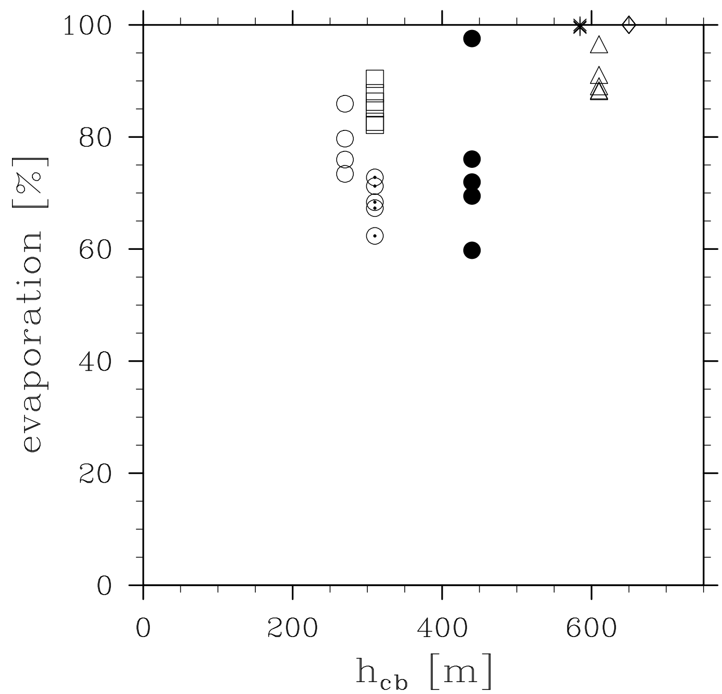

Figure 14: Evaporation of drizzle in the subcloud layer defined as ($R_{radar,cb}$ -$R_{radar,sfc}$)/$R_{radar,cb}$ as a function of mean cloud base height h_{cb}. Each point represents one flight leg of approximately 30 minutes. Symbol representation identical to Figure 7.

values up to roughly 0 dBz the relationships are within one standard deviation of the ones given in Table 2 while for higher $Z_{in\ situ}$ values they are within two standard deviations.

Table 5 also shows R-values derived using a $R - Z$ relationship based on all the nighttime flights (see Table 2). These values are lower than those in the first column of Table 5 but are within one standard deviation of the values in Table 1. Inclusion of the daytime flight, RF08, in the derivation of the $R-Z$ relationship (see Table 2) would induce large changes but based on just one flight it is not warranted to assign this to systematic day-night differences.

Both sensitivity tests - Table 1 vs. Table 5, and the two columns of Table 4 - indicate that the specific assumptions for the conversion of radar reflectivity to drizzle rate do not unduly influence the basic conclusions in Section 4.. The tests also indicate that the drizzle rates used in Section 4. are likely to be conservative.

While it is clear that it is difficult to make judgements about the absolute accuracy of the drizzle rates, it is worth emphasizing that in situ and radar-derived values are in reasonable agreement (*e.g.*, Figure 3, 9 and 10). Another set of R-Z relationships, derived using all in-cloud legs on a flight by flight basis, and using averages of observed droplet spectra (not fits) over 5-min periods, yielded $R_{radar,cb}$ values about a factor of two above those of Table 1 and a factor of five higher for RF02. These differences are larger than the uncertainty estimates derived in Section 3 in part due to not including in these latter estimates a stratification by height of the in-cloud spectra. Even so, the differences are (if RF02 is excepted) of the order of accuracy commonly connected with radar-

flight	drizzle rate no extrapolation [mm d^{-1}]	drizzle rate overall night Z-R [mm d^{-1}]
RF02	0.46 $\pm$ 0.17	0.27 $\pm$ 0.04
RF03	0.07 $\pm$ 0.05	0.06 $\pm$ 0.01
RF04	0.13 $\pm$ 0.12	0.11 $\pm$ 0.01
RF07	0.91 $\pm$ 0.34	0.73 $\pm$ 0.09
RF08	0.15 $\pm$ 0.04	0.09 $\pm$ 0.01

Table 5: Drizzle rates at 70 m height above the sea surface for the whole duration of each flight based on radar data. The conversion from radar reflectivity to drizzle rate is done with Z-R relationships derived from *in situ* instruments (SPP-100 and 260X) without extrapolation of the lognormal fit for each individual flight and with one generic relationship (based on all nighttime flights).

derived rainfall rates. The fact that the drizzle rate presented here might be on the low side only strengthens our conclusion about the prevalence and importance of drizzle in stratocumulus.

6. Summary

We have analyzed microphysical data obtained during the Dynamics and Chemistry of Marine Stratocumulus -II field study (DYCOMS-II). The field study consisted of nine flights with the NCAR C-130 aircraft in stratocumulus topped boundary layers and took place in July 2001 in the eastern Pacific region west-southwest of San Diego. Seven out of nine flights were flown during the night and seven out of nine flights consisted of a circular Lagrangian flight pattern. DYCOMS-II was blessed with favorable conditions: relatively uniform, and spatially extensive stratocumulus cloud decks were probed with few breaks. Thus, the visually uniform looking clouds hid rich differences in microphysical cloud structure.

The combined availability of the Wyoming cloud radar (Vali et al. 1998) and *in situ* microphysical instruments during the Dynamics and Chemistry of Marine Stratocumulus -II field study (DYCOMS-II, Stevens et al. 2003a) provided a unique opportunity to obtain estimates of drizzle rates in nocturnal marine stratocumulus. The results show that the prevalence of drizzle is higher than formerly thought. Out of seven flights analyzed, five had measurable mean precipitation at the surface, two with a substantial amount.

The drizzle rates have been estimated with respect to each flight, based on both *in situ* and remotely sensed data. Truncated lognormal functions have been fitted to the cloud droplet size distribution as measured by the SPP-100 and to the drizzle drop size distribution as measured by the 260X and 2D-C. Based on those fits, the drizzle rate R and reflectivity Z values have been calculated analytically over a diameter range up to 1 mm for each leg. Next, R-Z relationships were derived for each flight, both close to the surface and at cloud base height. Those relationships were used to convert Z_{radar} data at those two height levels into a rain rate. The radar measured Z close to the surface during all legs except the surface legs so an almost continuous estimate of the surface drizzle rate could be obtained. In this way a more accurate flight averaged drizzle rate can be estimated than one based on *in situ* data alone. Yet, the more intermittent results of the *in situ* instruments are also able to characterize the amount of drizzle of a particular flight very well (*i.e.*, indicate whether the drizzle rate is ‘very light’, ‘moderate’ or ‘heavy’), despite the inhomogeneity of the drizzle.

The general picture of drizzle in stratocumulus arising from the DYCOMS-II flights is one of large flight averaged drizzle rates being mainly due to the occurrence of localized patches of strongly enhanced precipitation. Together with low flight averaged drizzle rates correlating with a low intensity of drizzle this strongly suggests that drizzle could induce a transition in cloud structure (Stevens et al. (1998) and Paluch and Lenschow (1991)). Variability in drizzle rates among flights correlates well with cloud depth cubed divided by the total cloud droplet number, while variability in the *in situ* drizzle rate within each flight is explained by the variability in total drizzle drop number. Thus higher precipitation rates are not due to a change in shape of the drizzle drop distribution but are mainly caused by the appearance of larger drizzle drops - in the right tail end of the distribution - as a consequence of a higher total number of drizzle drops. Consequently, leg averaged *in situ* drizzle rates are well represented by values calculated by using leg averaged droplet distributions. On the macroscopic scale the drizzle rate also correlates negatively with ΔT (the difference between the 11 and 14 μm brightness temperatures as measured by the GOES-10 satellite), and shows signs as well of threshold-like dependence on *in situ* cloud top effective radius. Evaporation of drizzle in the subcloud layer is rather high, even for shallow boundary layers, and displays only a weak dependence on the depth of this layer.

Acknowledgments. Support by the National Science Foundation, through Grant # ATM 0097053 is gratefully acknowledged. For the first author this work is part of the research programme of the ‘Stichting voor Fundamenteel Onderzoek der Materie (FOM)’, which is financially supported by the ‘Nederlandse Organisatie voor Wetenschappelijk Onderzoek (NWO)’.

APPENDIX A
Fitting procedures

The first step in the fitting procedure is to calculate D_g and σ_g and N (see for the definition of these terms section 3 a.) from the data directly. The lognormal function specified by these values, however, is biased towards the higher moments, and in general, a better fit can be obtained by taking into account that the measured DSD's are truncated at both ends (defined as D_{min} and D_{max}). The so called truncated lognormal fit can be defined as the lognormal function having the same D_g and σ_g and N between D_{min} and D_{max} as the data. In Feingold and Levin (1986) analytical relationships are given between D_g and σ_g of the non-truncated lognormal function and the truncated lognormal function. To show the goodness of a certain fit it is common to use the so-called χ^2 test. χ^2 is defined as the ratio between the variance of the fit s^2 and the variance of the data σ^2 multiplied by the degrees of freedom $\nu = n - m$, with m the number of parameters (in our case equal to 3) used to fit a function to n data points.

The variance of the fit s^2 is given by:

$$s^2 = \frac{1}{\nu}\Sigma\frac{1/\sigma_i^2}{1/N\Sigma 1/\sigma_i^2}[N_i - f(D_i)]^2, \qquad (3)$$

with i the index representing the bin-number of the DSD. Once the χ^2 value is known, a statistical measure of goodness of fit can be determined by assuming that the errors in the data points are normally distributed. A rough estimate whether a fit is statistically 'good' or not can be obtained by comparing χ^2 and ν; for comparable values of the two the fit is acceptable. The applied length of the intermediate averaging period of 20 s is based upon this because σ^2 calculated from 6 20 s averages ensures a statistically good fit. While taking the standard deviation based upon one averaging period of 120 s gives a value for $\chi^2 << 1.$, indicating an overestimation of the variance in the data (Bevington and Robinson 1992)

Besides a statistical measure of the goodness of fit, uncertainty estimates for the fitting parameters should be given. We determined rough estimates of those uncertainties by variation of χ^2 round its local minimum:

$$\sigma = \Delta a\sqrt{\frac{2}{\chi_1^2 - 2\chi_2^2 + \chi_3^2}}, \qquad (4)$$

with a one of the fitting parameters and χ_i^2 the value of χ^2 for a_1, $a_2 = a_1 + \Delta a$ and $a_3 = a_2 + \Delta a$. It is important to realize that this uncertainty estimate σ should be interpreted as the variation needed in a to increase the minimum value of χ^2 by 1. (Bevington and Robinson 1992).

So after the calculation of the truncated fitting parameters the value of χ^2 is calculated, together with an estimate of the uncertainty in the three fitting parameters. The calculations of the uncertainties in the parameters supply six other χ^2 values, comparison of these values show that the truncated lognormal fit is often (more often for the CDSD's than for the DDSD's) but not always the fit with the lowest value for χ^2, *i.e.*, the best fit available. Despite this the values of the fitting parameters of the truncated lognormal fit are taken because it is the fit which conserves the moments of the data and in general the values of the fitting parameters would vary only slightly if the absolute best fit was taken. (Another reason not to always trust the χ^2 method is the fact that in the derivation of the least square method the assumption is made that uncertainties in the data are normally distributed, which may not be the case for the DSD which might suffer from more under sampling at the larger bin sizes.)

Because drizzle drops have a small incident rate some caution is necessary when fitting a DSD. In order to ensure enough counts in a sufficient number of bins the 1 second data of the SPP-100, 260X and the 2DC are averaged over 120 s. The length of this period is an optimum between reduction of the sampling error and conservation of the temporal and spatial scales. The lower limit for the necessary number of counts in one bin is 5, this number is often taken as one of the requirements to be able to classify a distribution as Gaussian instead of Poisson. However, bins with 4 counts or less are not disregarded despite the violation of the Gaussian distribution assumption. This is justified because almost all the bins with 4 counts or less are for the larger drop diameters and the fitting parameters are not sensitive to leaving out quite a number of bins of the largest drops. On the other hand the parameters are sensitive to the opposite; reducing the number of bins by removing bins with small drop diameters. This is easily understood when one realizes that the bins with small diameter generally contain the most counts, thus contributing most to the moments of the DSD. In order to fit two lognormal functions to the two physical modes instead of to the DSDs of the two different instruments, the fit to the CDSD is subtracted from the data of the DDSD (only for the region in which the measurements overlap) before fitting the latter.

During the fitting procedure bad convergence of the fit is encountered on several occasions. To deal with this several steps are taken. First of all, the data is always checked for the presence of enough bins for a fit; all DSD's with less than 10 bins containing data are disregarded. If there are enough bins but the convergence is bad, adjustments are made to the left or right limit, because sometimes the behavior at the DSD limits complicates the fitting. In all cases the fitting procedure is disregarded if the number of bins becomes too small to ensure a good fit. And if the convergence is still unsatisfactorily after these two corrections, the fitting procedure is abandoned and no fit is calculated.

References

Ackerman, A. S., O. B. Toon, P. V. Hobbs et al., 1993: Dissipation of marine stratiform clouds and collapse of the marine boundary layer due to the depletion of cloud condensation nuclei by clouds. *Science*, **262**, 226–229.

Albrecht, B. A., 1989: Aerosols, cloud microphysics, and fractional cloudiness. *Science*, **245**, 1227–1230.

Aldous, D., 1999: Deterministic and stochastic models for coalescence (aggregation, coagulation): A review of the mean-field theory for probabilists. *Bernoulli*, **5**, 3–48.

Austin, P., Y. Wang, R. Pincus, V. Kujala et al., 1995: Precipitation in stratocumulus clouds: Observational and modeling results. *J. Atmos. Sci.*, **52**, 2329–2352.

Bevington, P. R. and D. K. Robinson, 1992: *Data Reduction and Data Analysis for the Physical Sciences*. McGraw-Hill, 328 pp.

Boers, R., J. B. Jensen, P. B. Krummel et al., 1996: Microphysical and short-wave radiative structure of wintertime stratocumulus over the Southern Ocean. *Quart. J. Roy. Meteor. Soc.*, **122**, 1307–1339.

Boers, R., J. B. Jensen, P. B. Krummel et al., 1998: Microphysical and short-wave radiative structure of stratocumulus over the Southern Ocean: Summer results and seasonal differences. *Quart. J. Roy. Meteor. Soc.*, **124**, 151–168.

Brenguier, J. L., T. Bourrianne, A. de Araujo Coelho, R. J. Isbert, R. Peytavi, D. Trevarin, P. Weschler et al., 1998: Improvements of droplet distribution size measurements with the fast-FSSP (forward scattering spectrometer probe). *J. Atmos. Oceanic Tech.*, **15**, 1077–1090.

Bretherton, C. S., P. Austin, S. T. Siems et al., 1995: Cloudiness and marine boundary layer dynamics in the ASTEX lagrangian experiment part II: Cloudiness, drizzle, surface fluxes, and entrainment. *J. Atmos. Sci.*, **52**, 2724–2735.

Brost, R. A., J. C. Wyngaard, D. H. Lenschow et al., 1982: Marine stratocumulus layers. part II: Turbulence budgets. *J. Atmos. Sci.*, **39**, 818–836.

Chen, C. and W. R. Cotton, 1987: The physics of the marine stratocumulus mixed layer. *J. Atmos. Sci.*, **44**, 2951–2977.

Duynkerke, P. G., P. J. Jonker, A. Chlond, M. C. vanZanten, J. Cuxart, P. Clark, E. Sanchez, G. Martin, G. Lenderink, J. Teixeira et al., 1999: Intercomparison of three- and one-dimensional model simulations and aircraft observations of stratocumulus. *Boundary-Layer Meteorol.*, **92**, 453–487.

Duynkerke, P. G., H. Zhang, P. J. Jonker et al., 1995: Microphysical and turbulent structure of nocturnal stratocumulus as observed during ASTEX. *J. Atmos. Sci.*, **52**, 2763–2777.

Feingold, G. and Z. Levin, 1986: The lognormal fit to raindrop spectra from frontal convective clouds in israel. *J. of Clim. and Appl. Meteor.*, **25**, 1346–1363.

Feingold, G., B. Stevens, W. R. Cotton, A. S. Frisch et al., 1996: The relationship between drop in-cloud residence time and drizzle production in numerically simulated stratocumulus clouds. *J. Atm. Sci.*, **53**, 1108–1122.

Ferek, R. J., J. T. Garrett, P. V. Hobbs, S. Strader, D. Johnson, J. P. Taylor, K. Nielsen, A. Ackerman, Y. Kogan, Q. Lu, B. A. Albrecht, D. Babb et al., 2000: Drizzle suppression in ship tracks. *J. Atm. Sci.*, **57**, 2707–2728.

Frisch, A. S., C. W. Fairall, J. B. Snider et al., 1995: Measurement of stratus cloud and drizzle parameters in ASTEX with a K-band doppler radar and a microwave radiometer. *J. Atmos. Sci.*, **52**, 2788–2799.

Gerber, H., 1994: New microphysics sensor for aircraft use. *Atmospheric Research*, **31**, 235–252.

Gerber, H., 1996: Microphysics of marine stratocumulus clouds with two drizzle modes. *J. Atmos. Sci.*, **55**, 1649–1662.

Han, Q., W. Rossow, R. Welch, A. White, J. Chou et al., 1995: Validation of satellite retrievals of cloud microphysics and liquid water path using observations from FIRE. *J. Atmos. Sci.*, **54**, 4183–4195.

Hocking, L. M., 1959: The collision efficiency of small drops. *Quart. J. Roy. Meteor. Soc.*, **85**, 44–53.

Khairoutdinov, M. and Y. Kogan, 2000: A new cloud physics parameterization in a large-eddy simulation model of marine stratocumulus. *Mon. Wea. Rev.*, **128**, 229–243.

Kogan, Y. L., M. P. Khairoutdinov, D. K. Lilly, Z. N. Kogan, Q. Liu et al., 1995: Modeling of stratocumulus cloud layers in a large eddy simulation model with explicit microphysics. *J. Atmos. Sci.*, **52**, 2293–2940.

Kraus, E. B., 1963: The diurnal precipitation change over the sea. *J. Atmos. Sci.*, **20**, 551–556.

Lasher-Trapp, S. G., W. A. Cooper, A. M. Blyth et al., 2002: Measurement of ultragiant aerosol particles in the atmosphere from the small cumulus microphysics study. *J. Atmos. and Oceanic. Tech.*, **19**, 402–408.

Nicholls, S., 1984: The dynamics of stratocumulus: Aircraft observations and comparisons with a mixed layer model. *Quart. J. Roy. Meteor. Soc.*, **110**, 783–820.

Nicholls, S., 1987: A model of drizzle growth in warm, stratiform clouds. *Quart. J. Roy. Meteor. Soc.*, **113**, 1141–1170.

Nicholls, S. and J. Leighton, 1986: An observational study of the structure of stratiform cloud sheets: Part I. structure. *Quart. J. Roy. Meteor. Soc.*, **112**, 431–460.

Paluch, I. R. and D. H. Lenschow, 1991: Stratiform cloud formation in the marine boundary layer. *J. Atmos. Sci.*, **48**, 2141–2158.

Pawlowska, H. and J.-L. Brenguier, 2003: An observational study of drizzle formation in stratocumulus clouds during ACE-2 for GCM parameterizations. *J. Geophys. Res.*, **99**, 999–999, in press.

Perez, J. C., F. Herrera, F. Rosa, A. Gonzales, M. Wetzel, R. Borys, D. Lowenthal et al., 2000: Retrieval of marine stratus cloud droplet size from NOAA AVHRR night imagery. *J. Rem. Sensing of Environ.*, **73**, 31–45.

Pincus, R. and M. B. Baker, 1994: Effect of precipitation on the albedo susceptibility of clouds in the marine boundary layer. *Nature*, **372**, 250–252.

Rogers, R. R. and M. K. Yau, 1989: *A short course in cloud physics*. Butterworth Heinemann, 290 pp.

Stevens, B., . co authors et al., 2003a: Dynamics and chemistry of marine stratocumulus -dycoms-II. *Bull. of Amer. Met. Soc.*, **84**, 579–593.

Stevens, B., W. R. Cotton, G. Feingold, C. H. Moeng et al., 1998: Large-eddy simulations of strongly precipitating, shallow, stratocumulus-topped boundary layers. *J. Atmos. Sci.*, **55**, 3616–3638.

Stevens, B., G. Vali, K. Comstock, R. Wood, M. C. vanZante, P. Austin, C. S. Bretherton and D. H. Lenschow, 2003b: Pockets of open cells (POCs) and drizzle in marine stratocumulus. *Science*, Submitted.

Vali, G., R. D. Kelly, J. French, S. Haimov, D. Leon, R. E. McIntosh, A. Pazmany et al., 1998: Finescale structure and microphysics of coastal stratus. *J. Atmos. Sci.*, **55**, 3540–3564.

Wang, S. and Q. Wang, 1994: Roles of drizzle in a one-dimensional third-order turbulence closure model of nocturnal stratus-topped marine boundary layer. *J. Atmos. Sci.*, **51**, 1559–1576.